ORF 94/5

# DEVELOPMENTS IN COMPUTER METHOD FOR FLUID-STRUCTURE INTERACTIONS

Richard Madden
John C. O'Callahan


NORTHEASTERN UNIVERSITY
Boston, Massachusetts 02115

August 31, 1969

NGR-22-011-042
NASA Grant. ~~NGR-22011042~~

**FINAL REPORT**

Period Covered: August 1, 1968-July 31, 1969


Prepared for

NATIONAL AERONAUTICS AND SPACE ADMINISTRATION

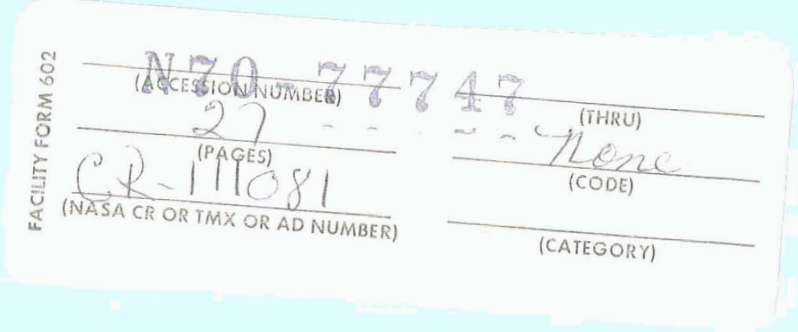

# DEVELOPMENTS IN A COMPUTER METHOD FOR FLUID-STRUCTURE INTERACTIONS

Richard Madden
John C. O'Callahan

NORTHEASTERN UNIVERSITY
Boston, Massachusetts 02115

August 31, 1969

NASA Grant. NGR-22011042

FINAL REPORT

Period Covered: August 1, 1968 - July 31, 1969

Prepared for

NATIONAL AERONAUTICS AND SPACE ADMINISTRATION

# DEVELOPMENTS IN A COMPUTER METHOD FOR FLUID-STRUCTURE INTERACTIONS

By Richard Madden and John C. O'Callahan
Northeastern University

## SUMMARY

A computer method has been developed for the analysis of the interaction of a fluid and a structure. The technique is a coupling of a method of characteristics solution of the inviscid, non-heat conducting, unsteady fluid dynamic equations in cylindrical coordinates and the solution of a set of equations for the structure. The method has been used to generate a computer program applicable to the determination of the flow field inside a rigid parachute configuration and the dynamic deflection of a circular linear membrane which has been placed into an initially uniform free stream. Plots are presented for the flow field inside the parachute and for the response of the membrane and the flow field at various times.

## INTRODUCTION

The present work presents results from the early stages of a program whose ultimate objective is the theoretical prediction of the fabric stresses in a deploying parachute. A complete theoretical analyses of this phenomenon has not as yet been attempted due to the complexity of the fluid-structure interaction. Analyses have therefore been constrained to simplified models for either the structure or the fluid dynamics. For example, a recent theoretical analysis, ref. 1, has assumed a simple model for the flow field inside the canopy and concentrated on the material behavior. Peak stresses from this analysis compare favorably with the limited set of experimental results, however, the simplified aerodynamic model may not be applicable to some of the other problems of interest. This deficiency has been recognized in ref. 1.

Another pertinent analysis has been presented in ref. 2. This paper presents the results from a computer program for analyzing the aerodynamics inside a rigid cup shaped body. The results compare well with experimental values for pressure on the cup. The method, however, relies on a transformation of the region between the shock and the cup which may be difficult to apply for the configurations encountered during parachute inflation.

The present approach is designed to incorporate both a good representation of the flow field and a model for the parachute. The program is not as yet sufficiently advanced to handle parachutes, however, it has been used to analyze the interaction of an initially uniform free stream on a linear membrane and to give values for the resulting flow field and membrane deflections.

The method utilizes a pair of computer programs which were developed separately and then coupled implicitly. The aerodynamic computer program solves the inviscid non-heat conducting unsteady fluid dynamic equations in cylindrical coordinates by utilizing an approach based on the method of characteristics. The approach is similar to that developed in ref. 3. The structure, here assumed to be a membrane, is also solved using finite difference techniques. The present method is sufficiently general so that any structural model may be substituted for the membrane by merely changing one subroutine.

## SYMBOLS

| | |
|---|---|
| $C$ | isentropic sound speed |
| $C_p$ | pressure coefficient |
| $E$ | function of entropy |
| $F$ | arbitrary function |
| $h$ | time step |
| $h_r$ | spacing between points on membrane |
| $N$ | tension per unit length of membrane |

| | |
|---|---|
| $P$ | pressure |
| $r$ | radial coordinate |
| $s$ | entropy |
| $t$ | time |
| $U$ | radial velocity |
| $\overline{U}$ | velocity normal to boundary |
| $V$ | axial velocity |
| $\overline{V}$ | velocity tangential to boundary |
| $W$ | membrane deflection |
| $Z$ | axial coordinate |
| $\alpha$ | angle between r and $\xi$ axes |
| $\beta_i$ | $= \frac{1}{2}(\psi o + \psi i)$ |
| $\gamma$ | ratio of specific heats |
| $\Delta P$ | pressure difference across membrane |
| $\eta$ | tangential coordinate to boundary |
| $\theta$ | angle between projection of inward normal to bicharacteristic on r, z, plane and r axis. |
| $\overline{\theta}$ | $= \theta - \alpha$ |
| $\xi$ | normal coordinate to boundary |
| $\rho$ | fluid density |
| $\rho_*$ | surface density of membrane |
| $\sigma$ | $= P^{\frac{\gamma - 1}{2\gamma}}$ |
| $\psi$ | $= \frac{2}{\gamma - 1}\sqrt{\gamma E^{1/2}}$ |

Subscripts:

| | |
|---|---|
| f | free stream |
| i | i th bicharacteristic |
| m | membrane |
| o | updated time plane |
| p | particle path |

## GOVERNING EQUATIONS

The complete model of a fluid interacting with a membrane requires the general governing equations describing the motion of the membrane and the fluid together. Obtaining an exact solution to this set of equations with their associated coupled, time dependent, boundary conditions would be a formitable, if not impossible task. Therefore, it seems advisable to approach this problem numerically by developing separate computer programs and then coupling them through the boundary conditions. This requires a model for the fluid and a model for the membrane. The models utilized in the present approach are discussed in the following sections.

### Fluid Model

The unsteady inviscid axisymmetric equations are used to model the fluid portion of the interaction. These equations may be written as follows:

Continuity:

$$\frac{D\rho}{Dt} + \rho\left(\frac{\partial U}{\partial r} + \frac{\partial V}{\partial z} + \frac{U}{r}\right) = 0 \tag{1a}$$

Radial momentum:

$$\rho\frac{DU}{Dt} + \frac{\partial P}{\partial r} = 0 \tag{1b}$$

Axial momentum:

$$\rho\frac{DV}{Dt} + \frac{\partial P}{\partial z} = 0 \tag{1c}$$

Conservation of entropy along a particle path:

$$\frac{DP}{Dt} - c^2 \frac{D\rho}{Dt} = 0 \qquad (1d)$$

Equation of state:

$$P = P\ (\rho, s) \qquad (1e)$$

where:

$$\frac{D}{Dt} = \frac{\partial}{\partial t} + U \frac{\partial}{\partial r} + V \frac{\partial}{\partial z}$$

and $\rho$ is the density, P the pressure, s the entropy, r and U the radial coordinate and velocity, respectively; z and V the axial coordinate and velocity, respectively; t the time, and c is the isentropic sound speed.

Equation (1d) is used to eliminate the $\rho$ derivative in the continuity equation producing:

$$\frac{DP}{Dt} + \rho c^2 \left( \frac{\partial U}{\partial r} + \frac{\partial V}{\partial z} + \frac{U}{r} \right) = 0 \qquad (2)$$

The application of the method of characteristics to equations (1) and (2) yields two sets of characteristic equations (see for example, ref. 3), particle paths which are surfaces of possible discontinuity in the entropy derivative and the usual bicharacteristic equations. Each set is composed of a slope and compatability equation.

Slope equations along particle paths:

$$\frac{dr}{dt} = U \ ; \ \frac{dz}{dt} = V \qquad (3)$$

Bicharacteristics:

$$\frac{dr}{dt} = U + c \cos \theta \ ; \ \frac{dz}{dt} = V + c \sin \theta \qquad (4)$$

where $\theta$ is the angle measured between the projection of the inward normal to the bicharacteristic onto the r, z plane and the r axis.

Compatibility equation along particle paths:

Equation (2) may be utilized as a compatibility relationship along a particle path.

Compatibility equation along bicharacteristics:

$$\frac{dP}{dt} + \rho c \cos\theta \frac{dU}{dt} + \rho c \sin\theta \frac{dV}{dt} = -\rho c^2 S \tag{5}$$

where $\frac{d}{dt}$ represents the total derivative along a bicharacteristic:

$$\frac{d}{dt} = \frac{D}{Dt} + c \cos\theta \frac{\partial}{\partial r} + c \sin\theta \frac{\partial}{\partial z}$$

and:

$$S = \sin^2\theta \frac{\partial U}{\partial r} - \sin\theta \cos\theta \left( \frac{\partial U}{\partial z} + \frac{\partial V}{\partial r} \right)$$

$$+ \cos^2\theta \frac{\partial V}{\partial z} + \frac{U}{r}$$

An alternate form of equations (2) and (5) can be obtained using the perfect gas relation:

$$P = E(s) \rho^{\gamma}$$

And defining:

$$\psi = \frac{2}{\gamma - 1} \sqrt{\gamma E^{\frac{1}{\gamma}}} \quad \text{and} \quad \sigma = P^{\frac{\gamma-1}{2\gamma}}$$

where E is a function of entropy and $\gamma$ is the ratio of specific heats.
The second form of the compatibility equations then becomes:

$$\psi \frac{d\sigma}{dt} + c \left( \frac{\partial U}{\partial r} + \frac{\partial V}{\partial z} + \frac{U}{r} \right) = 0 \tag{6}$$

$$\psi \frac{d\sigma}{dt} + \cos\theta \frac{dU}{dt} + \sin\theta \frac{dV}{dt} = -c S \tag{7}$$

When a point is in the vicinity of a physical boundary, it is convenient to use normal ($\xi$) and tangential ($\eta$) coordinates with respect to the physical boundary and therefore, equations (6) and (7) may be written as:

$$\psi \frac{d\sigma}{dt} + c \left( \frac{\partial \overline{U}}{\partial \xi} + \frac{\partial \overline{V}}{\partial \eta} + \frac{U}{r} \right) = 0 \tag{8}$$

$$\psi \frac{d\sigma}{dt} + \cos\overline{\theta} \frac{d\overline{U}}{dt} + \sin\overline{\theta} \frac{d\overline{V}}{dt} = -c \overline{S} \tag{9}$$

where $\overline{\theta} = \theta - \alpha$ is the characteristic angle measured from the membrane normal, $\alpha$ is the angle between the r and the $\xi$ axis, and $\overline{U}$ and $\overline{V}$ are the normal and tangential velocities to the membrane, respectively:

$$\overline{S} = \sin^2 \overline{\theta} \frac{\partial \overline{U}}{\partial \xi} - \sin \overline{\theta} \cos \overline{\theta} \left( \frac{\partial \overline{U}}{\partial \eta} + \frac{\partial \overline{V}}{\partial \xi} \right)$$

$$+ \cos^2 \overline{\theta} \frac{\partial \overline{V}}{\partial \eta} + \frac{U}{r}$$

and: $\overline{U} = U \cos\theta + V \sin\theta$

$\overline{V} = V \cos\theta - U \sin\theta$

NOTE: the $\frac{U}{r}$ term is unchanged in the transformation of coordinates.

These equations, which are similar to those in ref. 4, are used to generate the finite difference equations.

The boundary conditions on the fluid are that the radial velocity at the axis of symmetry is zero and that the velocity of a fluid particle adjacent to a physical boundary is zero relative to the boundary.

The initial condition for the fluid portion of the problem, will depend upon the particular problem under consideration and therefore these will be presented in the results section.

## Membrane Model

The membrane is assumed to be a shallow axisymmetric shell which is restricted to small deflections. The partial differential equation of motion is, then:

$$N \left( \frac{\partial^2 W}{\partial r^2} + \frac{1}{r} \frac{\partial W}{\partial r} \right) + \Delta P = \rho_* \frac{\partial^2 W}{\partial t^2} \qquad (10)$$

where N is the tension per unit length of membrane, W the normal deflection, $\rho_*$ the material surface density, and $\Delta P$ the pressure difference across the membrane.

The boundary conditions on the membrane are that it is fixed at its outer edge and that the slope is zero at the origin. The pressure difference across the membrane is obtained from the fluid dynamic analysis.

## FINITE DIFFERENCE EQUATIONS

### Fluid Model

The finite difference equivalents of equations 3, 4, 6, 7, 8, and 9 are given as follows:

Slope equations along

Particle Paths:

$$r_p = r_o - U_p h \tag{11a}$$

$$z_p = z_o - V_p h \tag{11b}$$

Bicharacteristics:

$$r_i = r_o - (U_i + C_i \cos \theta_i) h \tag{12a}$$

$$z_i = r_o - (V_i + C_i \sin \theta_i) h \tag{12b}$$

Compatibility equations along

Particle paths:

$$\beta_5 \sigma_o + \frac{1}{2} c_o h \left( \frac{\partial U}{\partial r} + \frac{\partial V}{\partial z} + \frac{U}{r} \right)_o = K_5 \tag{13}$$

Or:

$$\beta_5 \sigma_o + \frac{1}{2} c_o h \left( \frac{\partial \overline{U}}{\partial \xi} + \frac{\partial \overline{V}}{\partial \eta} + \frac{U}{r} \right)_o = K_5 \tag{14}$$

Where:

$$K_5 = \beta_5 \sigma_5 - \frac{1}{2} c_5 h \left( \frac{\partial U}{\partial r} + \frac{\partial V}{\partial z} + \frac{U}{r} \right)_5$$

And:

$$\beta_5 = \frac{1}{2} (\psi_o + \psi_5)$$

Bicharacteristics:

$$\beta_i \sigma_o + \sin \theta_i V_o + \cos \theta_i U_o + \frac{1}{2} C_o h \left[ \sin^2 \theta_i \frac{\partial U}{\partial r} - \sin \theta_i \cos \theta_i \left( \frac{\partial U}{\partial z} + \frac{\partial V}{\partial r} \right) + \cos^2 \theta_i \frac{\partial V}{\partial z} + \frac{U}{r} \right]_o = K_i \tag{15}$$

Or:

$$\beta_i \sigma_o + \sin \bar{\theta}_i \bar{V}_o + \cos \bar{\theta}_i \bar{U}_o + \frac{1}{2} C_o h \left[ \sin^2 \bar{\theta}_i \frac{\partial U}{\partial \xi} - \sin \bar{\theta}_i \cos \bar{\theta}_i \left( \frac{\partial \bar{U}}{\partial \eta} + \frac{\partial \bar{V}}{\partial \xi} \right) + \cos^2 \bar{\theta}_i \frac{\partial \bar{V}}{\partial \eta} + \frac{U}{r} \right]_o = K_i \qquad (16)$$

Where:

$$K_i = \beta_i \sigma_i + \cos \theta_i U_i + \sin \theta_i V_i - \frac{1}{2} C_i h S_1$$

$$S_i = \left[ \sin^2 \theta \frac{\partial U}{\partial r} - \sin \theta \cos \theta \left( \frac{\partial U}{\partial z} + \frac{\partial V}{\partial r} \right) + \cos^2 \theta \frac{\partial V}{\partial z} + \frac{U}{r} \right]_i$$

$$\beta_i = \frac{1}{2} (\psi_o + \psi_i)$$

$$C_o = \frac{1}{2} (\gamma - 1) \psi_o \sigma_o$$

In these equations, h is the time step; subscript o represents quantities in the updated time plane at which the solution is desired; subscripts i and p, represent values in the back time plane ($t_o$ - h) on the characteristic coniod and the particle path, respectively.

Equations (11) to (16) are written in a form which is accurate to the order of the time step squared. Equation (15) may appear at first to be of O ($h^3$), however, the angle $\theta$ is not allowed to vary along the bicharacteristic; and thus, the equation is of O ($h^2$). Additionally, equations (15) and (16) use positions in the back time plane which have been located accurate only to O ($h^2$), see equations (11) and (12). Therefore, equation (16) is also O ($h^2$). This scheme yields an explicit solution in contrast to the O ($h^3$) scheme which is implicit and therefore requires iterations. The computing time for this scheme is consequently much smaller than the pure O ($h^3$) scheme. The present set of equations does, however, involve information from both time planes, and therefore, may be expected to give better results, in areas of high gradients, than the usual O ($h^2$) scheme. It should be noted, however, that the accuracies quoted are for an individual time step. The final solution is reduced by one order after a number of time steps and therefore it is accurate to the order of the time step itself.

In general, equations (13) to (16) contain the seven unknowns, $\sigma_o$, $U_o$,

$(\frac{\partial U}{\partial r})_o$, $(\frac{\partial V}{\partial z})_o$, $(\frac{\partial U}{\partial z})_o$, $(\frac{\partial V}{\partial r})_o$, however, a proper selection of characteristic angles will eliminate some of the unknown derivatives. Once the required number of characteristics are selected, the equations may be solved for Po, Uo, Vo to yield values on a spacial grid superimposed on the flow field at each increment in time.

## SPACIAL DERIVATIVES

The spacial derivatives of the functions $K_5$, $S_i$ appearing in equations (13) to (16) are obtained from a Taylor expansion; for example, consider the derivative in the r direction of some artitrary function F.

$$F(r + \delta r, z) = F(r, z) + \delta r_1 \frac{\partial F}{\partial r}(r, z) + \frac{\delta r_1^2}{2} \frac{\partial^2 F}{\partial r^2}(r, z)$$

$$F(r - \delta r, z) = F(r, z) - \delta r_2 \frac{\partial F}{\partial r}(r, z) + \frac{\delta r_2^2}{2} \frac{\partial^2 F}{\partial r^2}(r, z)$$

where r, z is the point at which the derivative is desired and $\delta r_1$, $\delta r_2$ are the forward and backward derivative spacings respectively.
Solving for $\frac{\partial}{\partial r} F$ gives:

$$\frac{\partial F}{\partial r} = \frac{(\delta r_2)^2 F(r + \delta r_1, z) - (\delta r_1)^2 F(r - \delta r_2, z) - \left[(\delta r_2)^2 - (\delta r_1)^2\right] F(r, z)}{\delta r_1 \ \delta r_2 \ (\delta r_1 + \delta r_2)} \quad (17)$$

Similar expressions for other partial derivatives can be found accurate to the order of the derivative spacing squared. Note, equation (17) is applicable to forward and backward differences, as well as central differences. The forward and backward differences are required when the point at which the derivative is desired is near a boundary.

## MEMBRANE MODEL

The finite difference equivalent of equation (10) may be written as:

$$w_{k,\, j+1} = \frac{N}{\rho_*}\left[1 + \frac{1}{2(k-1)}\right]\left(\frac{h}{h_r}\right)^2 w_{k+1,\, j} + 2\left[1 - \frac{N}{\rho_*}\left(\frac{h}{h_r}\right)^2\right] w_{k,\, j}$$

$$\frac{N}{\rho_*}\left[1 - \frac{1}{2(k-1)}\right]\left(\frac{h}{h_r}\right)^2 w_{k-1,\, j} - w_{k,\, j-1} + \Delta P_{k,\, j} \frac{h^2}{\rho_*} \qquad K \neq 1 \qquad (18a)$$

$$w_{1,j+1} = 4\frac{N}{\rho_*}\left(\frac{h}{h_r}\right)^2 w_{2,j} + 2\left[1 - 2\frac{N}{\rho_*}\left(\frac{h}{h_r}\right)^2\right] w_{1,j}$$

$$- w_{1,j-1} + \Delta P_{1,j}\frac{h^2}{\rho_*} \qquad K = 1 \tag{18b}$$

where k represents the $k^{\underline{th}}$ nodal point and j represents the $j^{\underline{th}}$ time plane, h is the time step and $h_r$ is the spacial grid spacing.

The difference operators in equations (18) are written to the order of the grid spacing squared and to the order of the time step squared. Note, however, that similar to the fluid portion the order of error in the timewise direction is reduced by one after a number of time steps.

The local velocities of the membrane are then determined from a backward difference operator applied to the deflections.

$$V_{k,j+1} = \frac{3W_{k,j+1} - 4W_{k,j} + W_{k,j-1}}{2h} \qquad j \geq 0$$

$$V_{k,1} = \frac{2\,(W_{k,1} - W_{k,0})}{h} + \frac{1}{2}\left(\frac{\partial W}{\partial t}\right)_{t=0} \qquad j = 0$$

where $V_{k,j}$ is the instantaneous velocity of the $K^{\underline{th}}$ nodal point at the $j^{\underline{th}}$ time step.

Initial conditions must be prescribed for both the deflection and velocity on the membrane. The initial condition on velocity is used to define $W_{i,-1}$ for the initial time cycle as follows:

$$\frac{\partial W_{i\,o}}{\partial t} = \frac{W_{i,1} - W_{i,-1}}{2h_t} \tag{19}$$

A discussion of the topological aspects of the computer method together with the procedures for solving the fluid model equations and the coupling of the fluid and structure models is presented in the following sections.

## TOPOLOGICAL ASPECTS

A feature of the present method is that the computer program is able to sense a moving boundary, such as a parachute, and consequently, it is able to divide the fluid flow field into a number of non-interacting regions. For example, if an impervious parachute is under consideration, the flow on the inside and outside of the parachute does not interact except near the mouth and the vent. The method consists of approximating the parachute by a number of connected straight line segments whose positions are a function of time. The equation of one of these segments is used to decide on which side of the parachute a particular point lies. In this manner it is possible to insure that all points used in a spacial partial derivative approximation are on the same side of the parachute and also to insure that the entire numerical conoid of dependence of a point lies on the same side of the parachute. The technique is similar to that presented in ref. 3.

## SOLUTION OF FLUID FINITE DIFFERENCE EQUATIONS

The finite difference equations are solved at each time plane to yield values of the dependent variables on the physical discontinuity (parachute or membrane) and also at points on a rectangular grid superimposed on the flow field. The solution at various locations in the field requires the consideration of two classes of points: those that lie sufficiently far away from a discontinuity and hence have a full conoid of dependence, and those points that lie on or near a discontinuity and therefore have a partial conoid of dependence. The numerical representation of the equations and the procedures for handling these two classes of points are discussed in the following sections.

### Points Having a Full Conoid of Dependence

For points having a full conoid of dependence, four bicharacteristics and the particle path are required to approximate the conoid. The values for $\theta_i$ are chosen, equally spaced, to be 0, $\pi/2$, $\pi$, and $3\pi/2$, as shown on figure 1.

The values of $\theta_i$ are chosen from stability considerations. The calculation requires the choice of a point $(r_o, z_o)$ at which the solution is desired in the new time plane. The location $(r_i, z_i)$ in the previous time plane of the characteristics which pass through $(r_o, z_o)$ may then be determined from equations (11) and (12). It is possible to find a point $(r_i, z_i)$ for which $u_i$, $v_i$, and $c_i$ satisfy equations (11) and (12) since values of all dependent variables are specified on the grid and on the discontinuities in the previous time plane. However, the solution of equations (11) and (12) is complicated by the fact that there is no explicit relation tying $(r_i, z_i)$ to $(U_i, V_i, c_i)$ in a given time plane. It is therefore necessary to choose some trial location for a bicharacteristic $(r_i, z_i)$ and use an iterative procedure (such as the Newton-Raphson method) to determine the actual coordinates $r_i$ and $z_i$. Once the coordinates $r_i$ and $z_i$ are established, linear interpolation is performed between the four surrounding grid points (or discontinuities) in the r - z plane to determine the values for all the required dependent variables at $(r_i, z_i)$.

Substituting these values into the four compatibility equations and the particle path relation and reducing gives equations for Po, Uo, and Vo of the form.

$$A\,\sigma_o^2 + B\,\sigma_o + C = 0$$

$$U_o = \frac{C_6 - C_4\,\sigma_o}{C_5} \tag{21}$$

$$V_o = \frac{C_3 - C_1\,\sigma_o}{C_2} \tag{22}$$

where:

$$\sigma_o = P_o^{\frac{\gamma-1}{2\gamma}}$$

The equations for $P_o$, $U_o$, $V_o$, for all the types of points, considered, may be written in this form, however, the definition of the coefficients A, B, C, and $C_1 - C_6$ will be a function of the type of point considered. The appropriate coefficients are given in ref. 5.

## Points Having a Partial Conoid of Dependence

Points lying on a discontinuity: Points lying on a discontinuity in this analysis are of two types: points on the axis of symmetry, and points on the membrane or parachute.

Field points on the axis of symmetry: The solution is accomplished by a reflection technique; that is, the bicharacteristic angles $\theta = 0$ and $\pi$ are symmetrically placed with respect to the axis (see figure 1). Thus, the information obtained for bicharacteristic $\theta = \pi$ is also used for $\theta = 0$, in the pertinent equations. The numerical equations for points on the axis must be modified to account for the fact that on the axis the $\frac{U}{r}$ term becomes:

$$\left(\frac{U}{r}\right)_{r=0} = \frac{\partial U}{\partial r} \tag{23}$$

The equations for $P_o$, $U_o$, and $V_o$ are the same as equations (20), (21), and (22) with new definitions for the coefficients.

Points on the membrane or parachute: In this case the orientation of the membrane or parachute controls the portion of the conoid which lies in the appropriate region and the original set of $\theta = 0$, $\pi/2$, $\pi$, and $3\pi/2$ are not applicable. A routine has been designed to allow the program to find the bicharacteristic angles which correspond to the boundary. The appropriate bicharacteristics are then $\overline{\theta} = \phi$, $\phi - \pi/2$, $-\phi$, and $\pi/2 - \phi$ where $\phi$ is an angle measured from the normal to the discontinuity. (See figure 2) The angle $\phi$ is assumed to be 2/3 of the way between the normal and the bicharacteristic angle to the closest discontinuity. The compatibility relations utilized are equations (14) and (16) with the following modification.

Since the points are on a impervious membrane, the relative fluid velocity normal to the membrane will be zero. The velocity components of the membrane are known quantities and, therefore, the velocity of the fluid may be determined. The additional relationships needed are:

$$\overline{U} = \overline{U}_f - \overline{U}_m \tag{24}$$

$$\overline{V} = \overline{V}_f - \overline{V}_m \tag{25}$$

where all velocity components are measured in the $\xi$, $\eta$ reference; $\overline{U}$, $\overline{V}$ are the velocity components of the fluid relative to the membrane; $\overline{U}_f$, $\overline{V}_f$ the velocity components of the fluid; and $\overline{U}_m$, $\overline{V}_m$ the velocity components of the membrane.

The pressures and velocities are evaluated, in an inertial reference frame which moves at the velocity of the physical boundary at the point under consideration, by solving equations (20) and (22) with $\overline{V}$ substituted for V. Thus, the total motion of the fluid is obtained by adding the velocity of the boundary to the results of equations (20) and (22).

Points on the membrane or parachute and also on the axis of symmetry: The procedure here is basically the same as the previous section with the use of a reflection procedure (see figure 2). The reflection technique is used in a similar manner to the field points on the axis except that two points are now reflected with respect to the membrane normal. Additionally: the $\frac{U}{r}$ term must be modified as follows:

$$\left(\frac{U}{r}\right)_{r = 0} = \frac{\partial \overline{V}}{\partial \eta} \tag{26}$$

Since there are no relative velocity components at this point only equation (20) is required.

Points lying near a discontinuity: The procedure followed here is similar to that for points lying on a discontinuity except that the velocity normal to the discontinuity does not vanish and consequently one additional characteristic is required. The appropriate angles measured from the local normal to the membrane are $\overline{\theta}$ = $\pi/2$, $-\pi/2$, $\pi/4$, $-\pi/4$, and 0 (see figure 3). If the point is on the axis the reflection technique is again used.

## COUPLING OF FLUID AND STRUCTURE MODELS

The coupling of the computer programs for the fluid field and the membrane is done in an implicit manner. The steps in the coupling process for a given time cycle are as follows:

1. The deflection and velocity at each nodal point on the membrane are determined from the pressure differences across the membrane and local velocities on the membrane at the previous two time steps.
2. The pressures and velocities of the fluid particles adjacent to the membrane are calculated at the positions determined in the previous step.
3. Deflections and velocities on the membrane are again calculated using the average of the pressure at the beginning of the time cycle and the pressure calculated at the updated membrane positions.
4. Step 2 is repeated and a new value for the average pressure during the time step is computed. This average pressure is compared with the average pressure used in step 3. A change in pressure less than or equal to 1% of the average pressure from step 3 is used as a criterion for convergence. If convergence is not established, steps 3 and 4 are repeated until convergence is attained or until a given amount of iterations has been exceeded. Exceeding of this limit will cause the program to stop.
5. The pressures and velocities are calculated at each point on the rectangular grid which has been superimposed on the flow field.

The maximum number of iterations for steps 3 and 4 has been set as 7, however, with the time step presently used no more than 2 iterations have been required.

## RESULTS AND DISCUSSION

A pair of cases are presented to illustrate the results of the present method. The first illustrates the flow in and around a parachute during some stage in its inflation and the second illustrates a fluid-structure interaction problem. In both the cases considered, the fluid is assumed as an ideal gas with $\gamma = 1.4$, free stream pressure of 14.7 lbs./in.$^2$, free stream velocity of 10,000 in./s, the spacial grid in the flow field was 3 in. by 3 in., and the time step h was $7.5 \times 10^{-5}$s. The time step is approximately 60% of the stability limit as predicted by the Courant Freidrichs & Lewy criterion for the free stream.

## Parachute Configuration

For this case, the parachute is assumed rigid and in the form of an O'Hara shape, as illustrated in figure 4. The O'Hara shapes provide a first order approximation to the geometry of an inflating parachute, by assuming that at each stage in the deployment the canopy may be represented by a combination of 2 simple geometrical shapes, a spherical section and a truncated conical section. In the numerical analysis, the canopy is approximated by a number of straight sided truncated conical segments.

The calculations were run on a 100 in. diameter parachute with an inlet diameter of 40 in. The canopy was assumed to be non-porous and it was not vented at the top. The parachute was represented by 10 points. The aerodynamic grid is 39 in. by 57 in. in the radial and axial directions respectively.

Figure (4b) is a section taken through the axis of symmetry of figure (4a). This figure shows the rigid parachute in the aerodynamic grid, the initial velocity distribution and the separated zone. The velocity, as shown in figure (4b), is assumed to be zero in the region above the lowest point on the parachute. The region below this is given an initial axial velocity $V_f$ of 10,000 in./s and zero radial velocity.

Flow separation is assumed to occur in the region downstream of the maximum radius of the parachute and the pressure in this region is taken to be ambient. Since the pressure is prescribed in this region, calculations are not performed outside the parachute downstream of its maximum radius.

A set of sample results is given in figures 5 to 8. These figures are copies of CALCOMP plots of the data from the computer program. Each figure illustrates the pressure on the parachute and the velocity at each point in the aerodynamic grid. The velocity is represented by a vector emanating from the point under consideration. The pressure on the parachute is plotted normal to the parachute. Velocity and pressure references are given on each figure for convenience.

The results for cycle 20 ($t = 1.5 \times 10^{-3}$s) are given in figure 5. One apparent difficulty that can be seen, however, is that the radial component of velocity is larger than expected in areas such as that outside the parachute. This results from a poor choice of boundary condition on the outermost radial grid, and has been fixed in the more recent version of the program. At this time, the velocity vectors and pressures indicate that the main pressure pulse has not quite reached the top of the parachute, and the pressures in this area are ambient. The small velocity vectors near the top of the parachute are due to numerical diffusion.

Figure 6 shows the flow field at the cycle 30 ($t = 2.25 \times 10^{-3}$s) just prior to reflection of the main pressure pulse from the top of the parachute, and the pressures have increased to approximately 29 psi near the top.

Figure 7 shows the flow field at cycle 40 ($t = 3.0 \times 10^{-3}$s) following the reflection of the main pressure pulse. The region near the top of the parachute is seen to be stagnated with velocities in this area due only to random numerical error.

Figure 8 shows the field at a still later time, cycle 45 ($t = 3.37 \times 10^{-3}$s) The stagnation region has grown over that of figure 7, however, a comparison of figures 7 and 8 shows that the pressures on the parachute are essentially the same and consequently equilibrium may be assumed to exist. These pressure distributions compare in form to those reported in ref. 6.

## Fluid-Membrane Interaction

The problem under consideration is the interaction of a uniform free stream of air and a 54 in. diameter membrane of mass per unit area $10^5$ lb. $s^2/in.^3$. The membrane is subjected to a uniform tension of 2125 lb./in. As shown in ref. 5, the numerical scheme will induce pressure transients in areas of severe gradients of pressure or velocity in the flow field. In order to eliminate the transients on the membrane, a starting solution has been used. This procedure allows part of the flow field to develop before the membrane is moved. The starting solution used assumes that the fluid particles on the membrane and one grid immediately in front

of the membrane are stagnated and have a pressure (39.75 lb./in.$^2$) obtained from a one-dimensional case where the fluid is stopped by the plate. The initial velocity of the membrane itself is assumed to be zero. This flow field corresponds physically to the case where a plug was placed behind the membrane to keep it rigid and then suddenly removed some time after the fluid struck the plate. See figure (9 ). The pressure on the upstream side of the membrane is maintained as ambient and calculations are not performed in this area.

Figure (10) presents the pressure on the axis of symmetry on the membrane as a function of time. In the initial few computational time cycles, a non-physical pressure rise occurs due to numerical diffusion. The pressure drop during the next few cycles is explained by the fact that as the membrane accelerates upwards, the fluid particles next to the membrane gain in velocity, thus, reducing their pressure. When the acceleration of the membrane becomes negative, the fluid particles are slowed down and consequently, the pressure rises again to a peak. The peak occurs just after the maximum deflection of the membrane. As the membrane moves in the opposite direction the pressure falls for the next few cycles. Following this, there is a dwell in pressure which will be discussed later with the aid of figures (13), (14), and (15). It results from the fact that as the membrane pushes fluid back into the flow field, it tends to swirl and form a low fluid velocity zone in front of the membrane. The pressure then decreases monotonically, with one slight bump, until a minimum is reached. This minimum occurs slightly later than the minimum deflection point. A scale for pressure coefficient $C_p$ is also shown on the plot. The pressure coefficient is seen to range from 3.2to 7.2during the first deflection cycle of the membrane.

Figure (11) illustrates the deflection of the membrane point on the axis as a function of time. This solution is compared with the solution which would have been obtained if the stagnation pressure of 39.75 lb./in.$^2$ had been used. Both curves are similar in shape, however, the constant pressure case has a larger maximum deflection and has a later time for the occurance of this maximum deflection. This is explained by the fact that in the interaction problem, the pressure on the membrane decreased as the membrane accelerates upward. The next minimum for the deflection is also lower than the interaction solution resulting from the fact that as the membrane returns, the pressure is above the stagnation pressure. It is, however, interesting to note that the ratio of the time between

maximum and minimum deflection to time for first maximum deflection is the same for both solutions. No explanation is offered for this, in fact, it may be fortuitous.

Figure (12) shows the deflected shapes of the membrane at various times. At t = .75 ms, the membrane is flat except near the outer edge since the signal that the boundary has zero deflection has not as yet reached the entire membrane. The curves for t = 1.5 and 1.8 ms show an almost first mode type shape as the membrane approaches its maximum deflection. The curve for t = 1.8 ms is in fact the maximum deflection. The curve for t = 4.2 ms is approximately at the minimum for the first cycle and is seen to be also in the first mode shape. This is, however, no guarantee that the membrane will continue to keep this shape for later cycles. In fact, it appears that there is a tendency for the last few cycles for the point on the axis to drop below its neighboring points thus indicating a contribution of the higher modes of vibration.

Figures (13), (14), and (15) illustrate the velocities in the fluid flow field and of fluid particles on the membrane at times t = 1.64, 2.1, and 3.0 ms. Figure (13) shows that at early times before maximum deflection, the flow field is directed towards the axis of symmetry as the fluid flows in to fill the additional area created by the deflecting membrane. Figure (14) illustrates the velocity vectors shortly after the point on the membrane on the axis has reversed direction and the membrane tries to push the fluid back into the free stream. Note, however, that the outermost points on the membrane are still traveling upwards and that the fluid in this area is traveling toward the axis. The fluid particles pushed back into the field by the membrane encounter forward moving fluid particles and consequently a swirl near the axis is created. The fluid in this swirl has a low velocity causing the pressure dwell noted in figure (10). Note also that there is a relative stagnation point on the membrane at the point where the inrushing fluid encounters the fluid being pushed out from the axis. The large values of radial velocity near the rigid wall on figure (14) and the next figure are caused by the fact that the edge of the computational grid is too close to the edge of the membrane and may easily be fixed by enlarging the computational grid. Figure (15) illustrates a later time when the stagnation point on the membrane has moved out to the edge of the membrane and the entire membrane is now

pushing fluid back into the main stream. The figures illustrate velocity vectors only part way into the flow field since the velocities below this are approximately free stream and consequently would be out of the scale for the present plots.

## CONCLUDING REMARKS

A numerical method of analysis for determining the interaction of a fluid and a structure has been developed and programmed. The method is part of the early stage of development of a computer program for analyzing the stresses in an inflating parachute. The method is based on an analysis of the flow field using concepts from the numerical method of characteristics coupled implicitly with an analysis of the dynamic response of a linear membrane. The approach is unique in that provisions have been made to recognize boundaries, such as a parachute, in the flow field and consequently physically non-interacting regions may be differentiated.

The method has been used to generate flow fields in and about a rigid shape which approximates a parachute during some stage in its deployment and also to analyze the interaction of a membrane and a uniform free stream.

## REFERENCES


1. Asfour, K. J.: Analysis of Dynamic Stress in an Inflating Parachute. J. Aircraft AIAA, Vol. 4, 5; Sept. - Oct., 1967.

2. Bastianon, R. A.: Unsteady Solution of the Flowfield Over Concave Bodies. AIAA J., Vol. 7, 3; Mar.1969.

3. Madden, R.: Hypervelocity Impact Analysis by the Method of Characteristics. NASA TR R-298, 1969.

4. Butler, D. S.: The Numerical Solution of Hyperbolic Systems of Partial Differential Equations in Three Independent Variables. Proc. Roy. Soc. Ser., A, Vol. 255; 1960.

5. O'Callahan, John C.: An Application of the Method of Characteristics to an Inviscid Fluid Interacting with an Initially Flat Circular Membrane. Northeastern Univ., Ph.D. Thesis; Aug. 1969.

6. Performance of and Design Criteria for Deployable Aerodynamic Decelerators. ASD-TR-61-579; Dec., 1963.

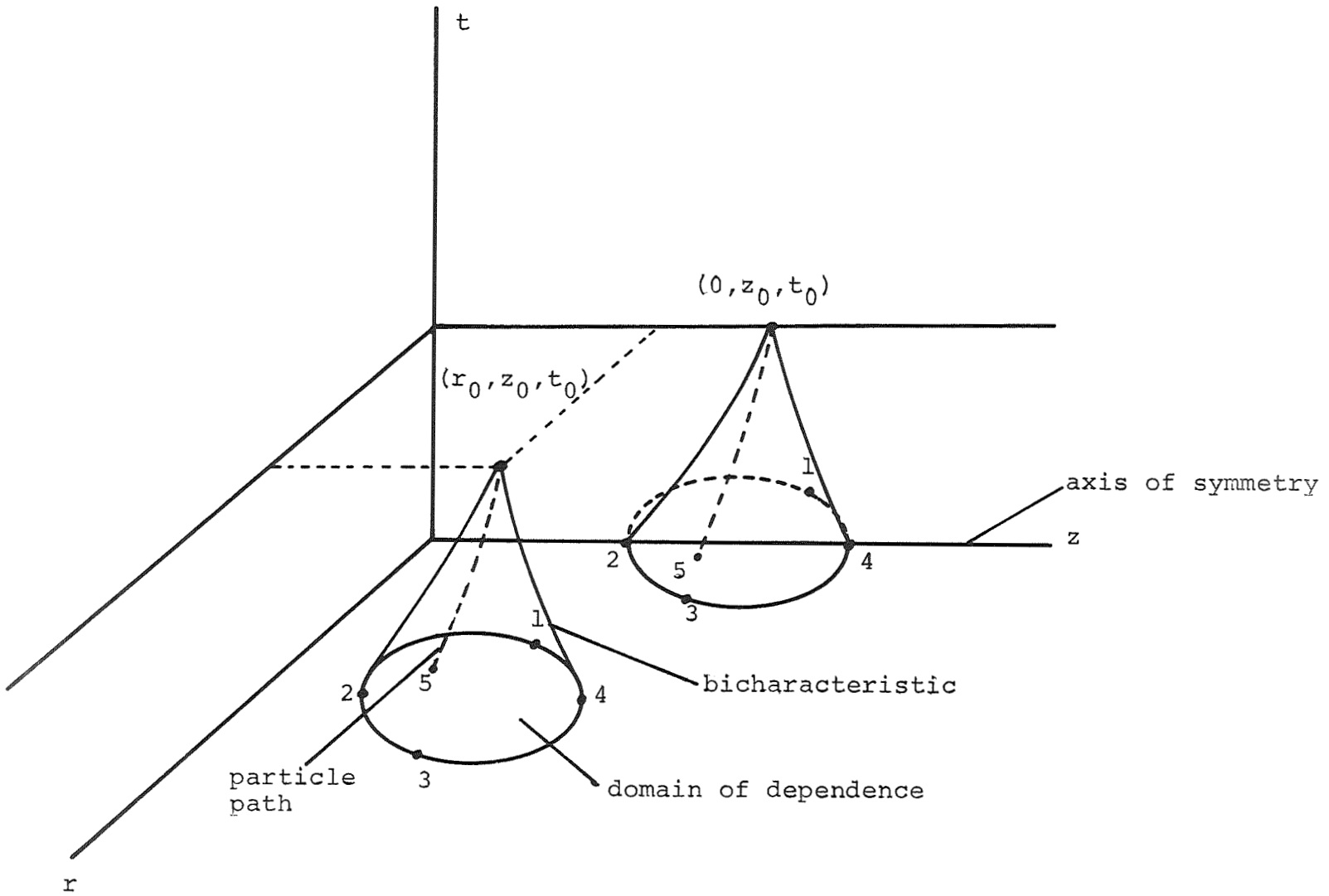


Figure 1 - Flow Field Conoids of Dependence

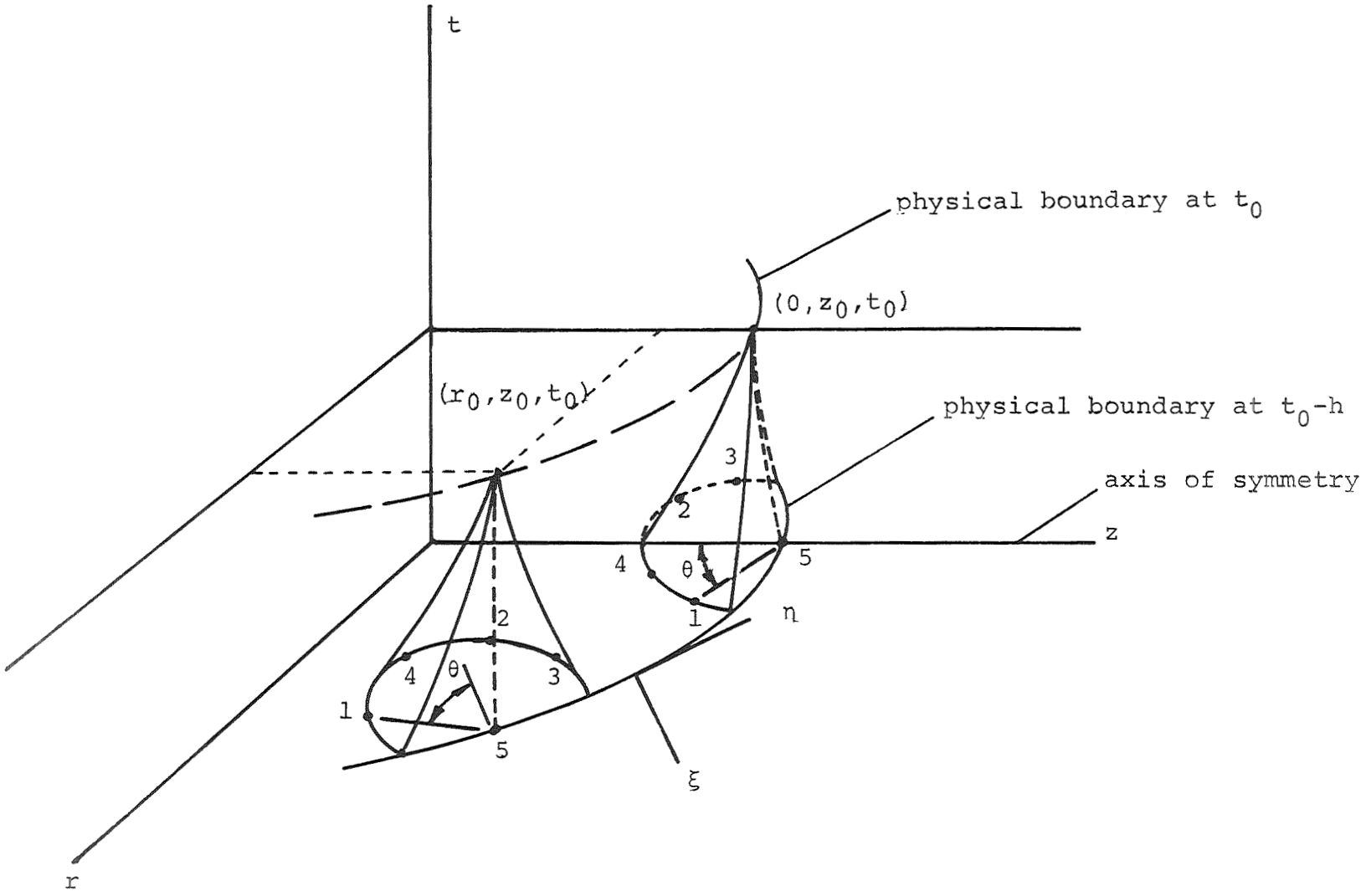


Figure 2 - Partial Conoids - Points on the physical boundary

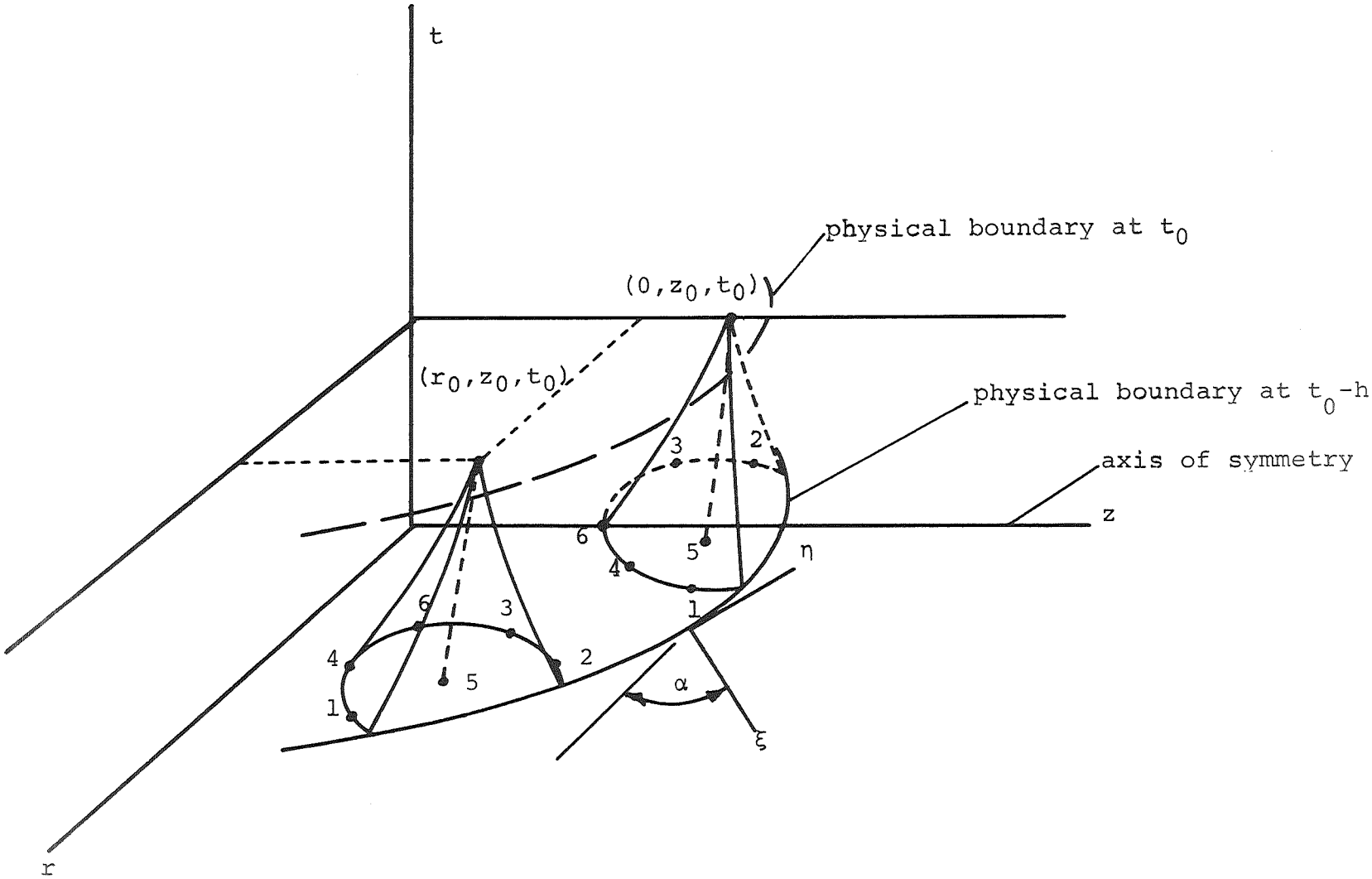


Figure 3 - Partial Conoids - Points near a physical boundary

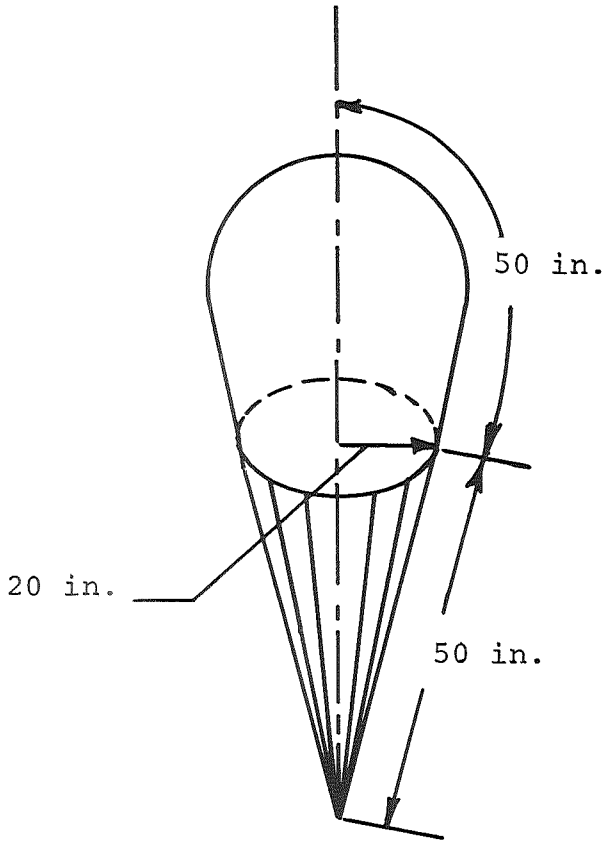


(a) Parachute Configuration

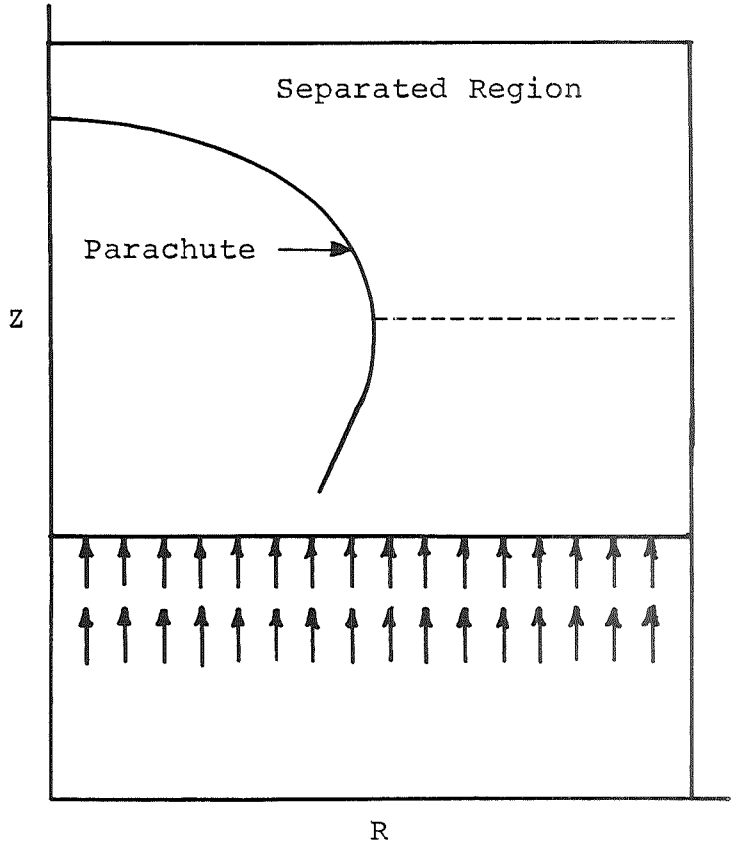


(b) Initial Conditions

Figure 4 - Parachute Configuration and Initial Condition

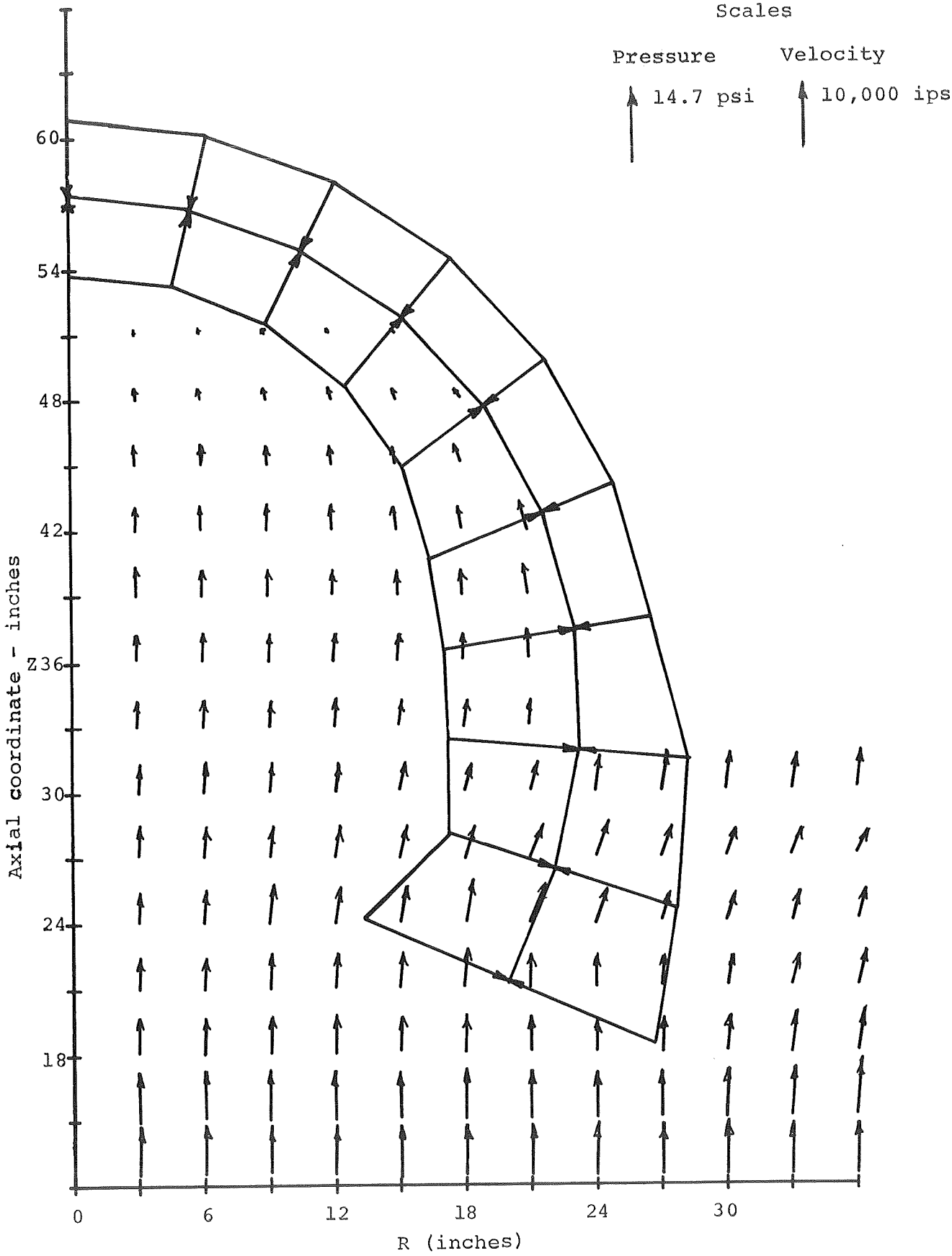


Figure 5 - Velocity field and pressure on parachute at computational cycle 20 for example problem.

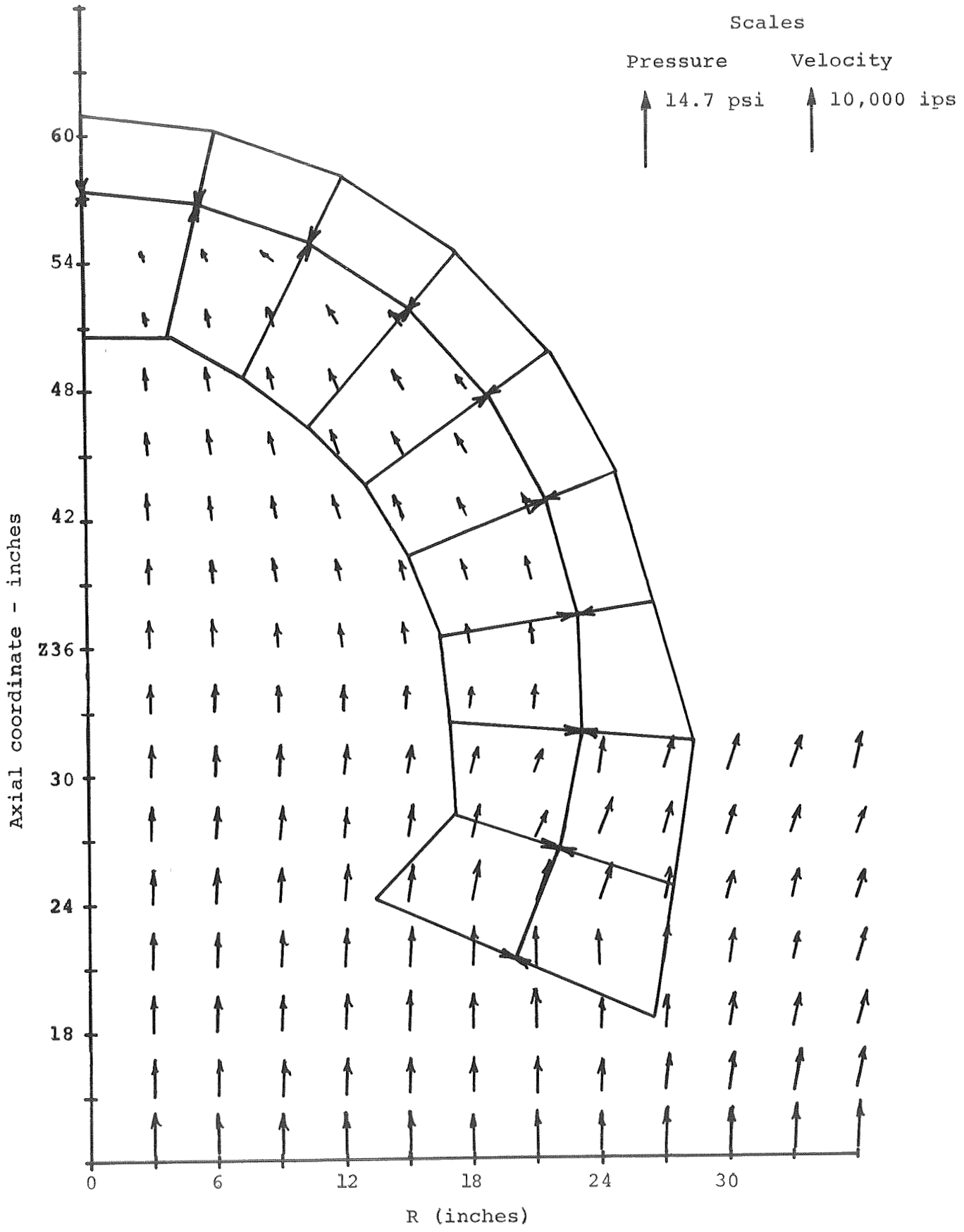


Figure 6 - Velocity field and pressure on parachute at computational cycle 30 for example problem.

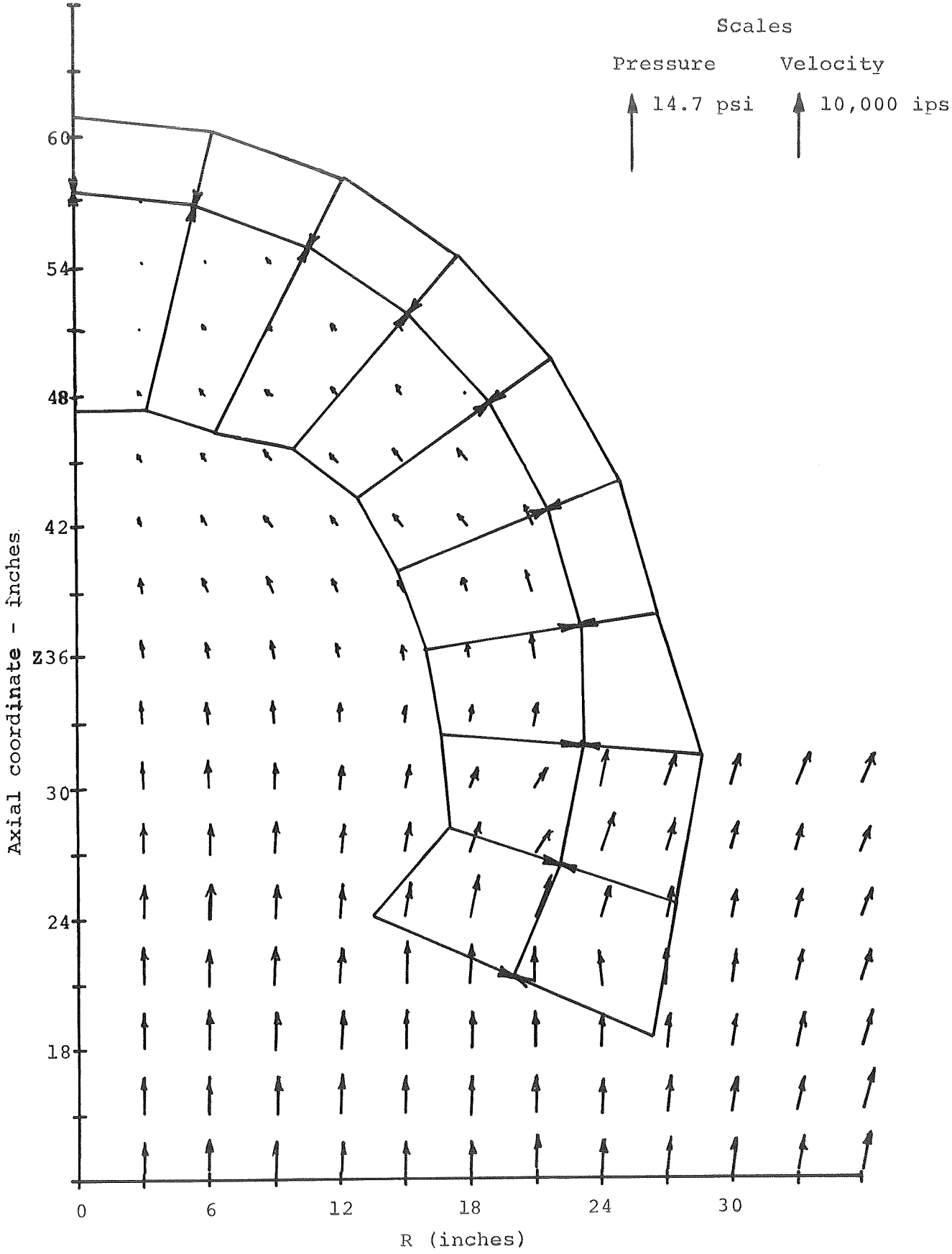


Figure 7 - Velocity field and pressure on parachute at computational cycle 40 for example problem.

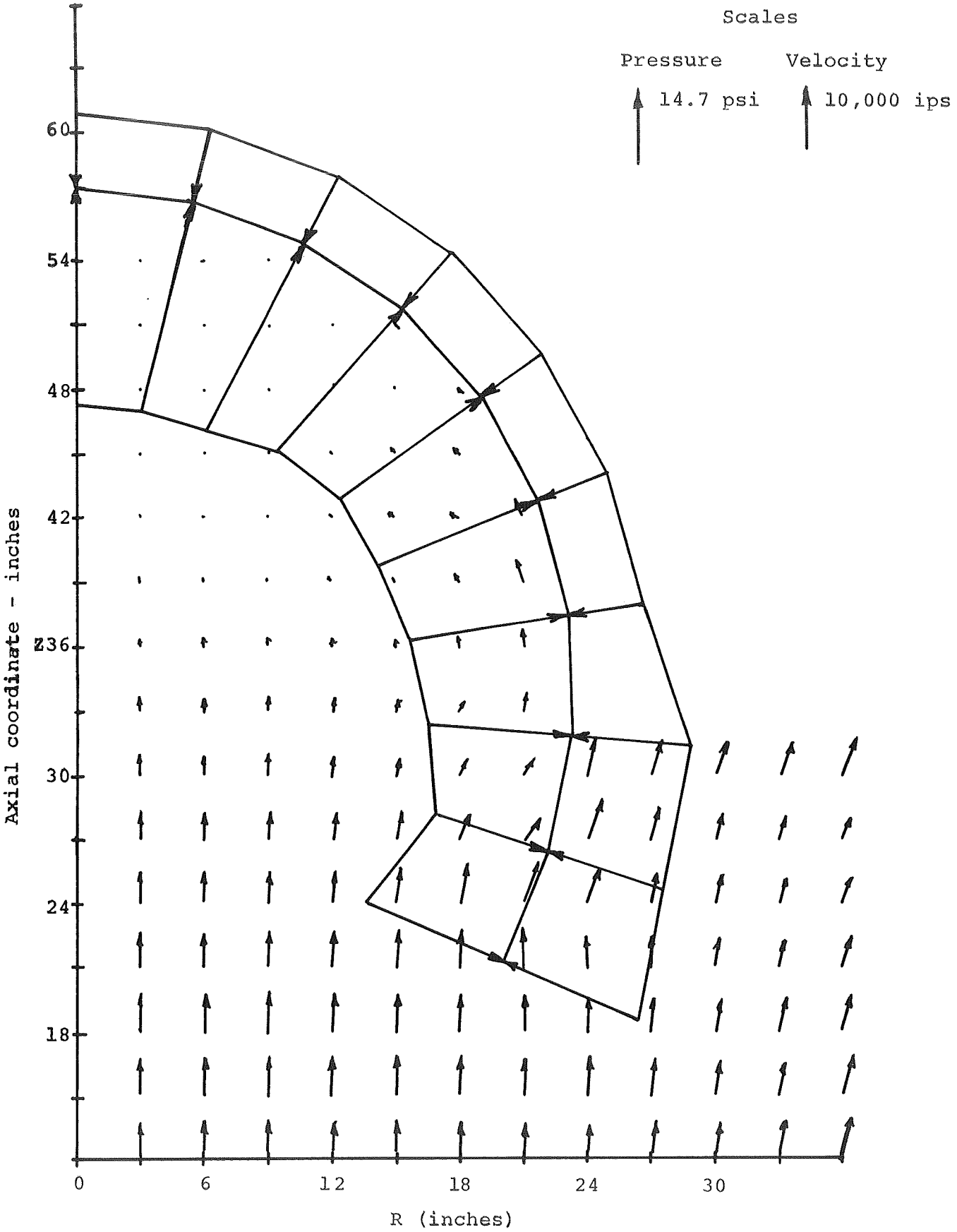


Figure 8 - Velocity field and pressure on parachute at computational cycle 45 for example problem.

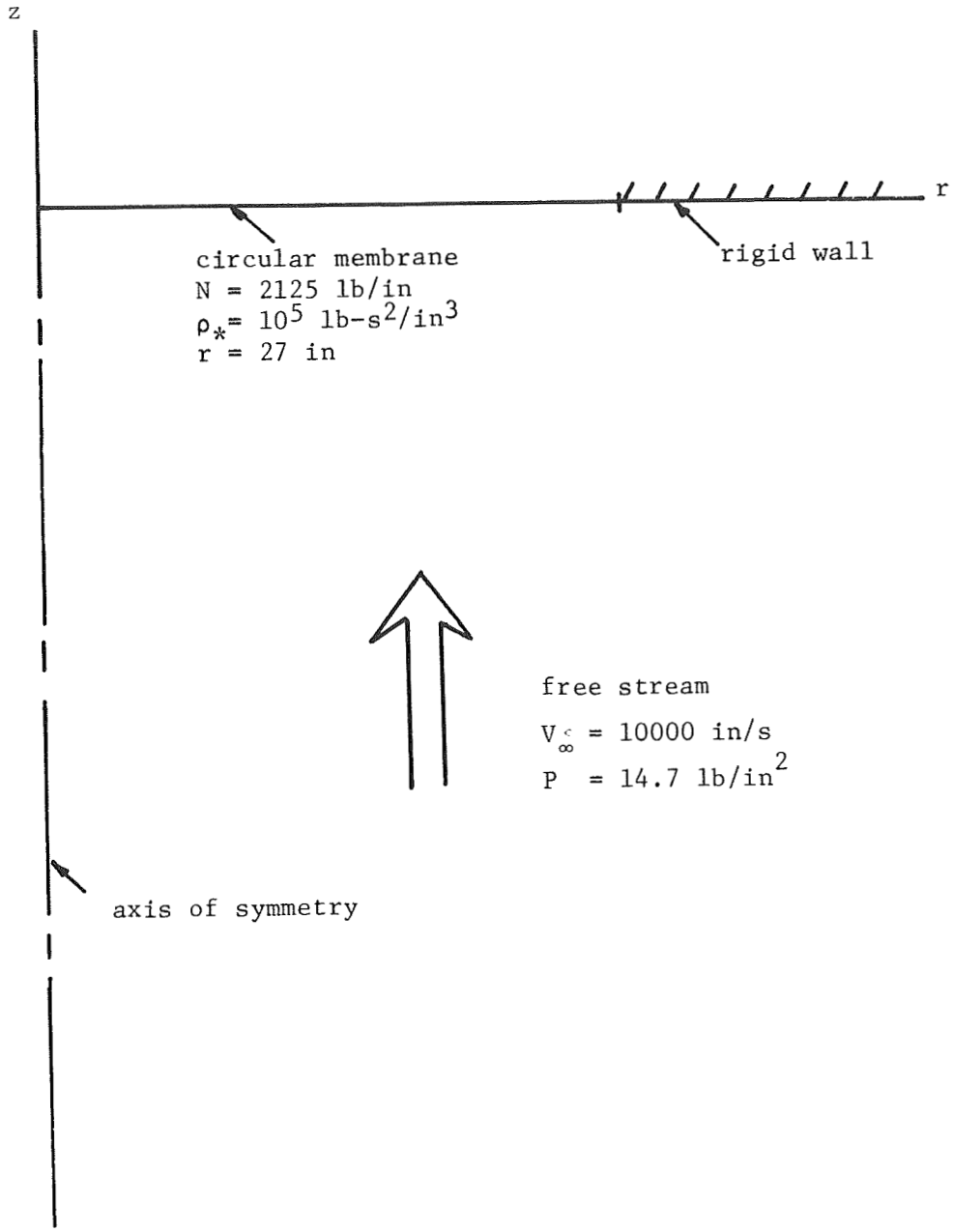


Figure 9 - Section through the axis of symmetry for the example fluid-membrane interaction.

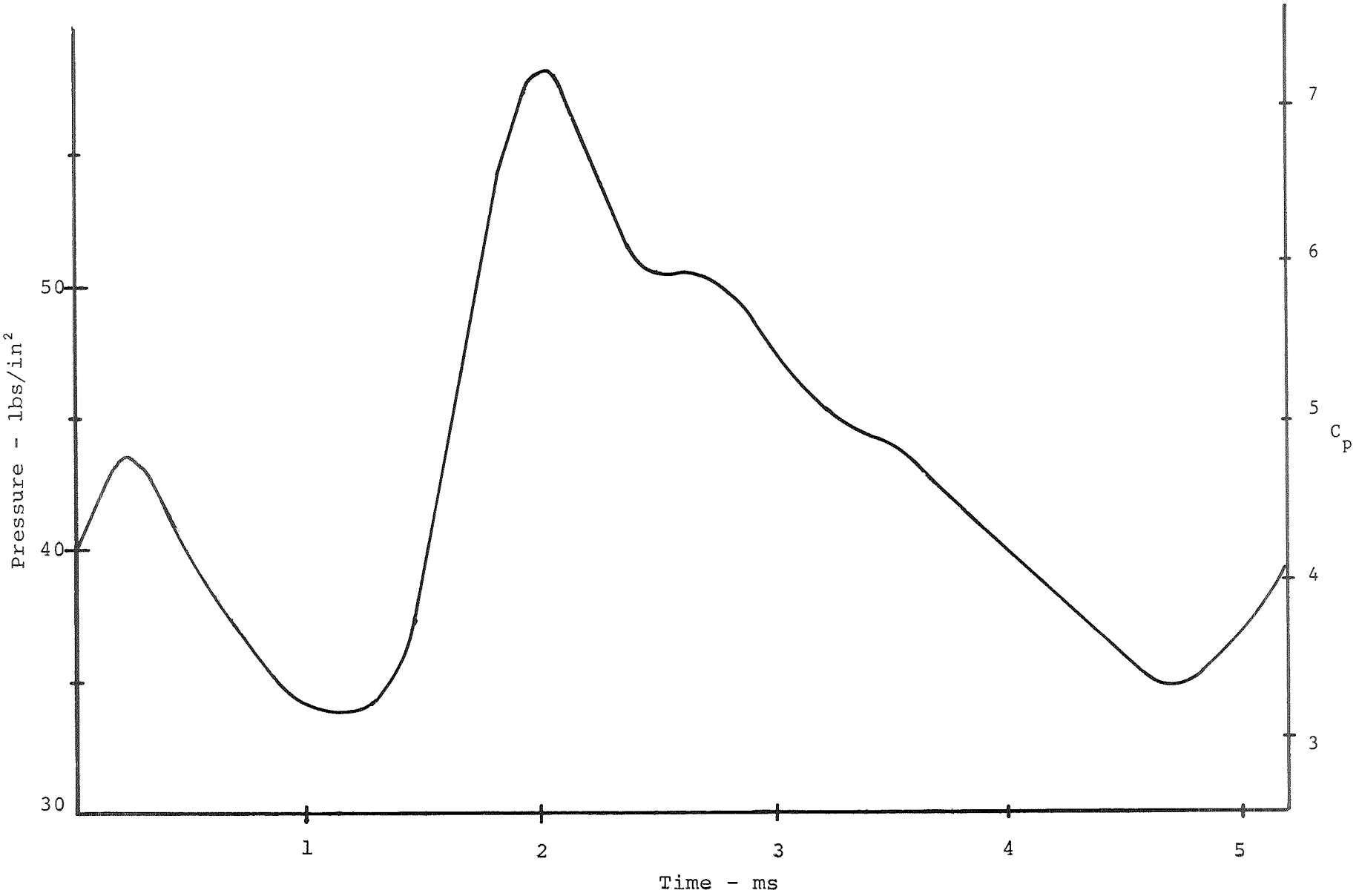


Figure 10 - Pressure at the membrane point on the axis of symmetry as a function of time for the example interaction problem.

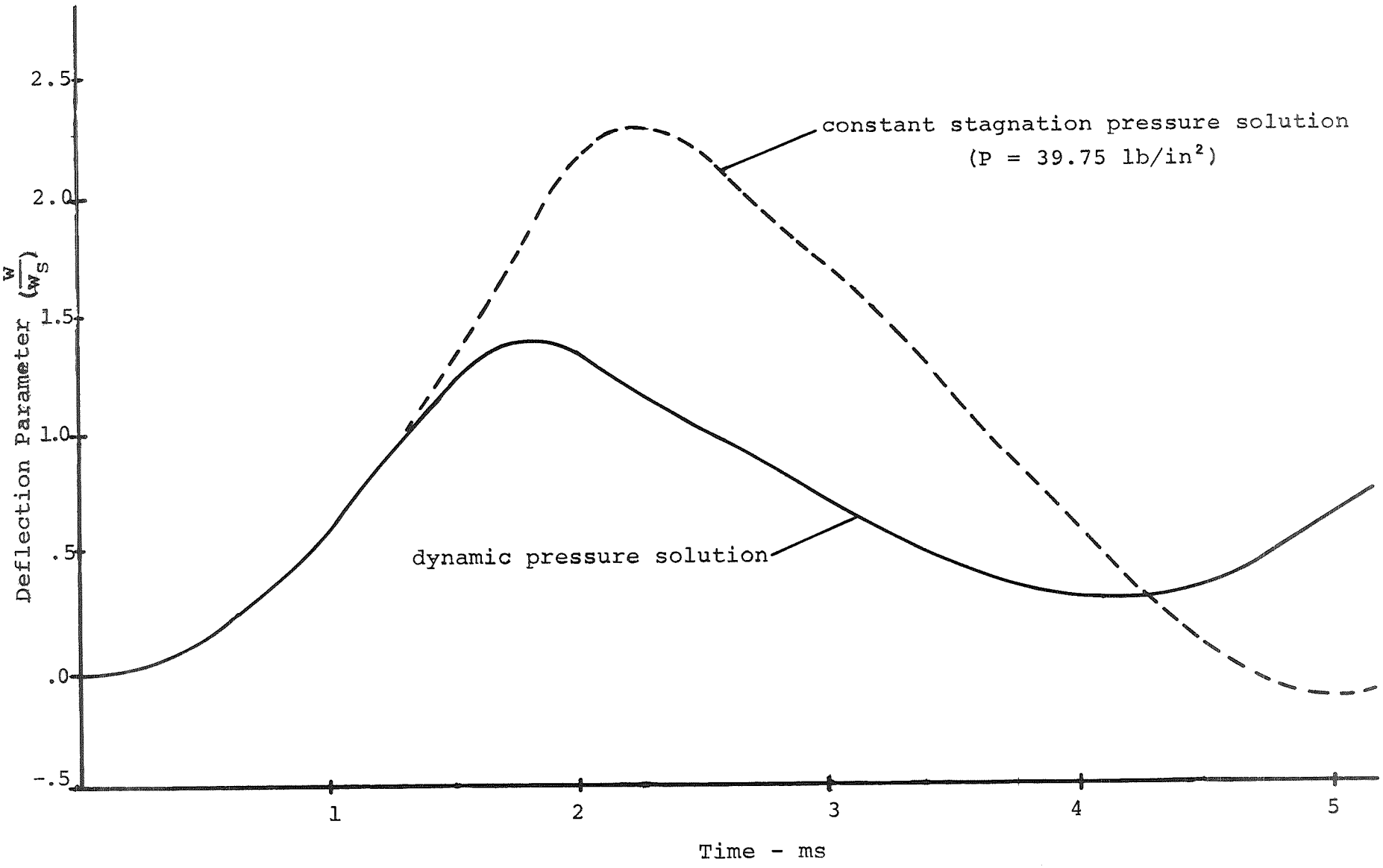


Figure 11 - Deflection of the membrane point on the axis of symmetry as a function of time for the example interaction problem.

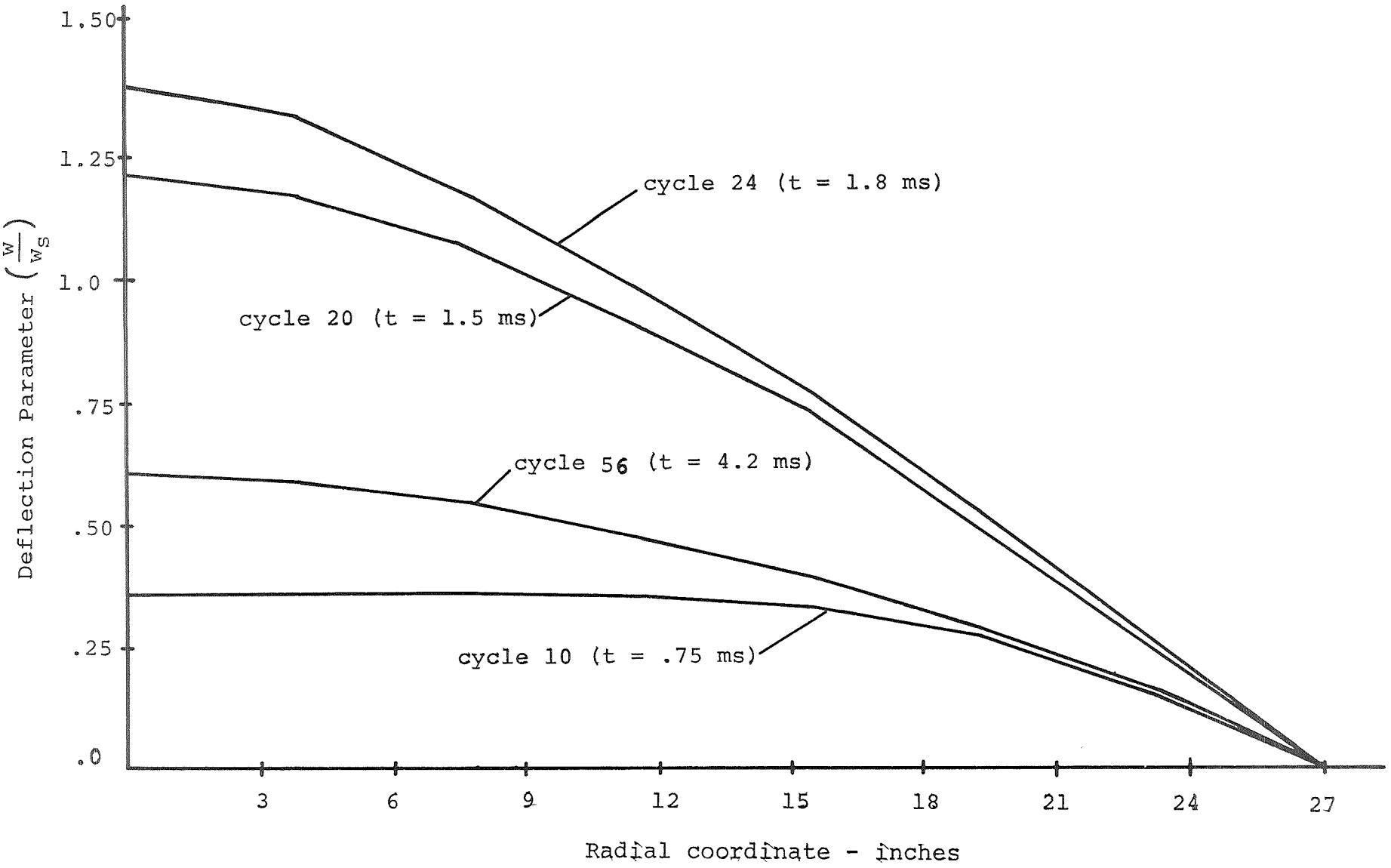


Figure 12 - Deflected shapes of the membrane at various times for the example interaction problem.

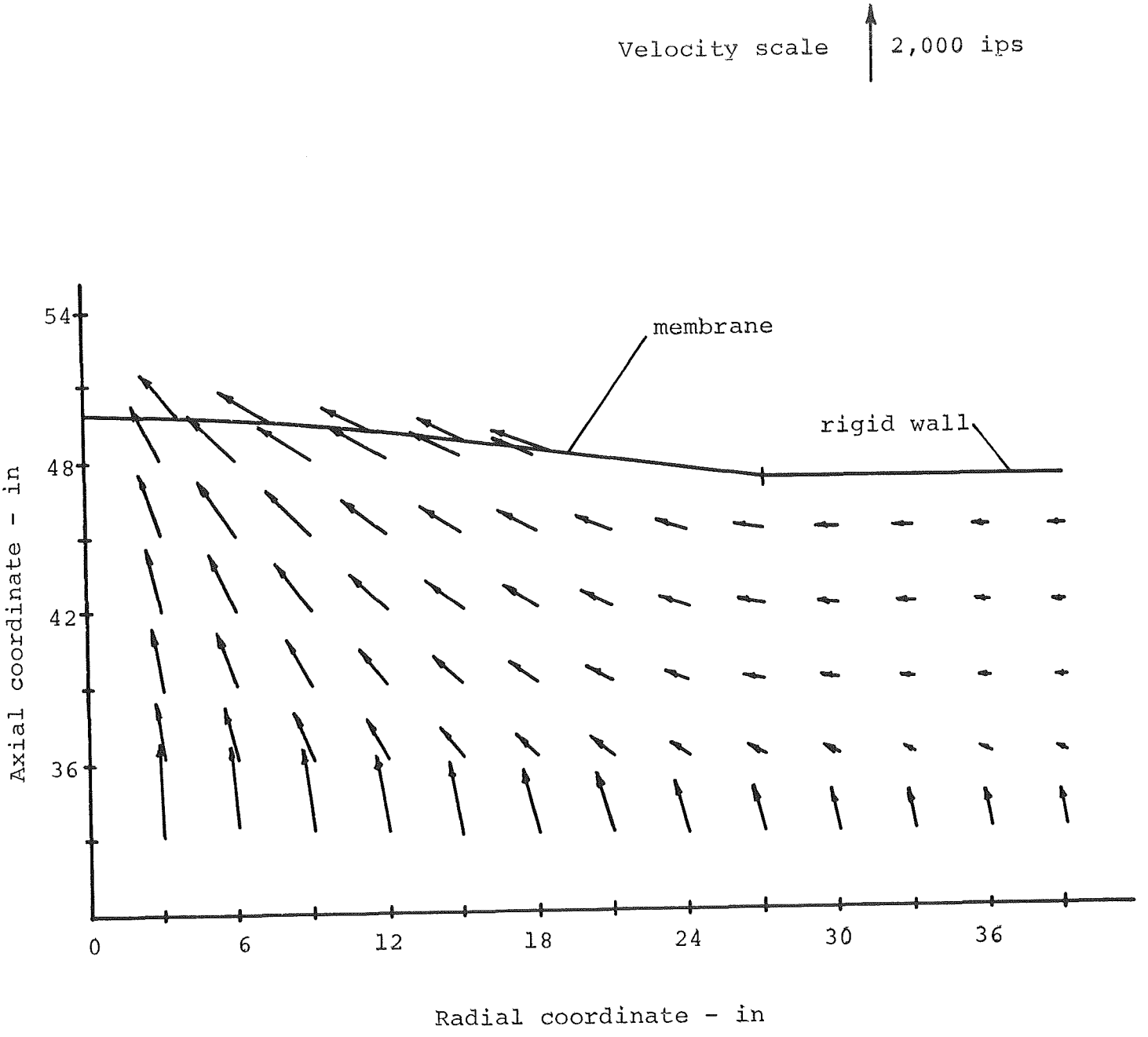


Figure 13 - Velocity field of the fluid below the membrane at cycle 22 (t = 1.64 ms), for the example interaction problem.

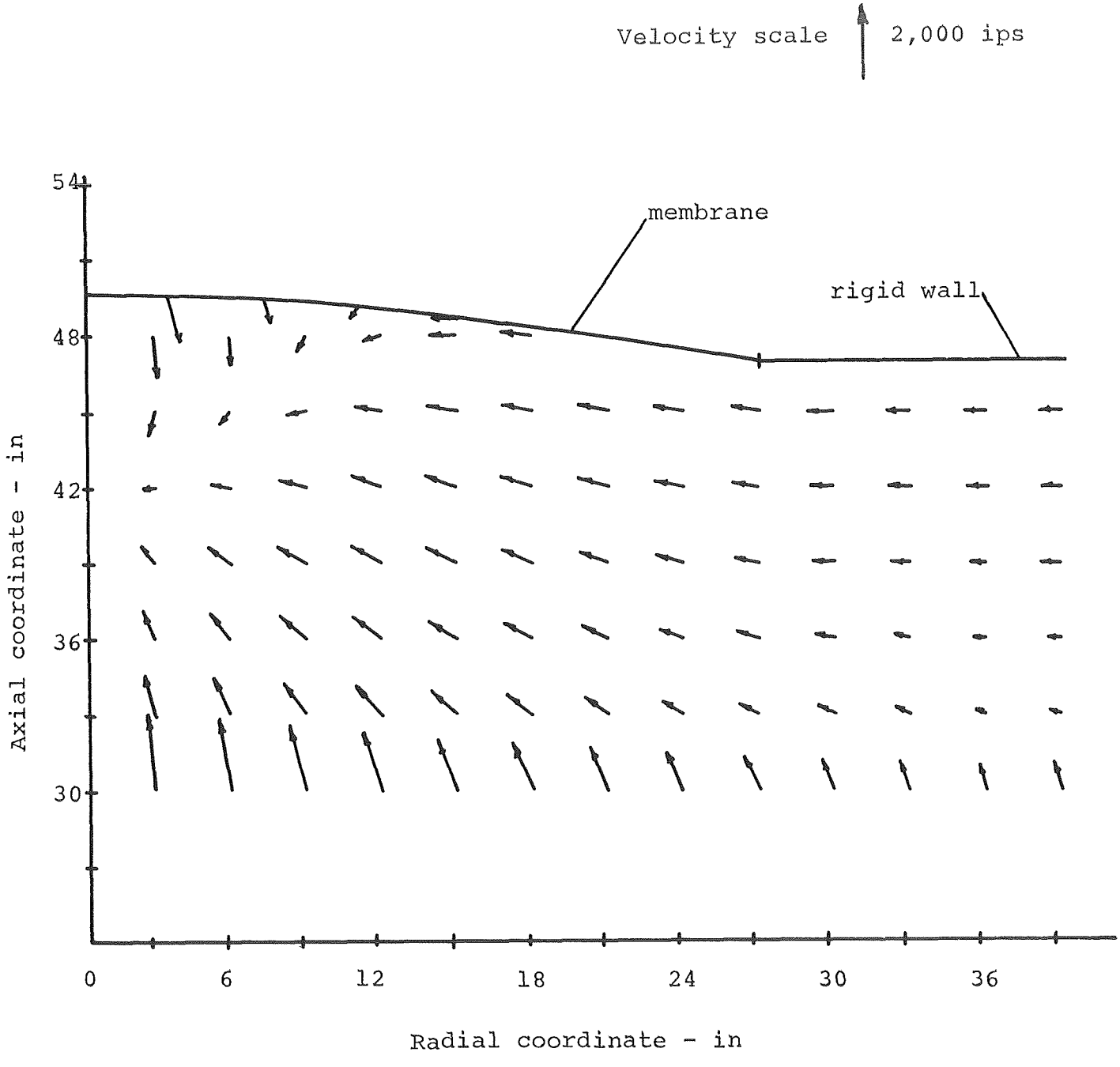


Figure 14 - Velocity field of the fluid below the membrane at cycle 28 (t = 2.1 ms), for the example interaction problem.

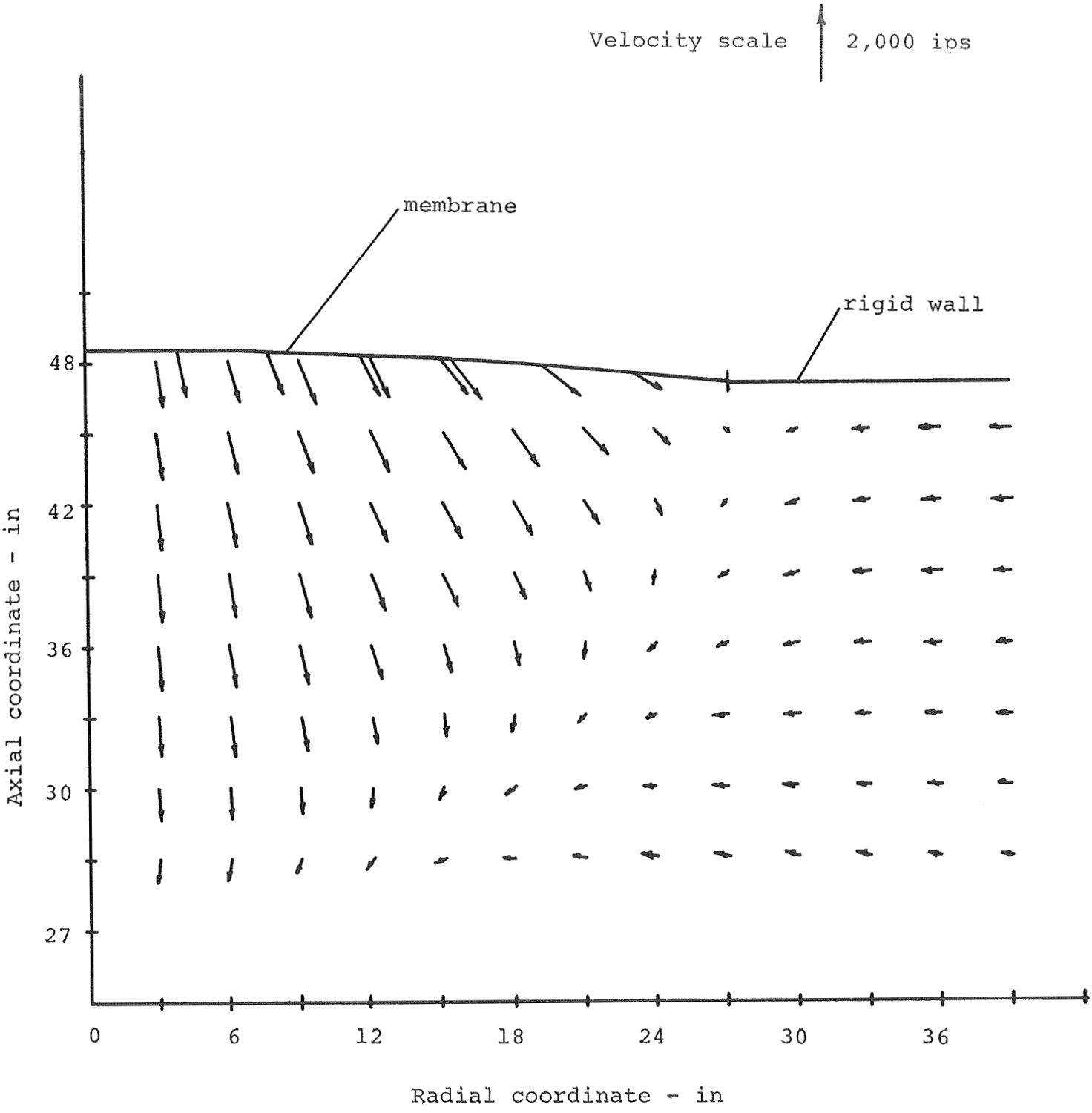


Figure 15 - Velocity field of the fluid below the membrane at cycle 40 (t = 3.0 ms), for the example interaction problem.